MULTI-DIMENSIONAL APPROACHES IN SEVERE ACCIDENT MODELLING AND ANALYSES

F. FICHOT*, O. MARCHAND, P. DRAI, P. CHATELARD, M. ZABIÉGO and J. FLEUROT
Institut de Radioprotection et de Sûreté Nucléaire
Direction de la Prévention des Accidents Majeurs
B.P.3 - 13115 Saint Paul Lez Durance, France.
*Corresponding author. E-mail : florian.fichot@irsn.fr

Received November 14, 2006

Severe accidents in PWRs are characterized by a continuously changing geometry of the core due to chemical reactions, melting and mechanical failure of the rods and other structures. These local variations of the porosity and other parameters lead to multi-dimensionnal flows and heat transfers. In this paper, a comprehensive set of multi-dimensionnal models describing heat transfers, thermal-hydraulics and melt relocation in a reactor vessel is presented. Those models are suitable for the core description during a severe accident transient. A series of applications at the reactor scale shows the benefits of using such models.

KEYWORDS : Severe Accident, Modeling, Heat Transfers, Thermalhydraulics, Melt Progression, Multi-dimensional, Porous medium

1. INTRODUCTION

After the Three-Mile Island accident, in 1979, research programs about severe accidents in nuclear reactors were initiated in many countries. It consisted in experiments, code developments and reactor studies which have led to a better understanding of the important physical processes involved during an accident scenario. It has also helped to define a "typical" accident progression. A severe accident occurs when a loss of coolant event is long enough to cause the core uncovery and a substantial degradation or even melting of the core assemblies. Therefore, one of the characteristic features of a severe accident is the progressive loss of geometry of the core.

The causes of deformation or degradation of fuel rods are numerous. For a low pressure scenario, initial deformations may be caused by the creeping of Zircaloy claddings due to the internal pressure of the fuel rods. At higher temperatures (above 1300K), the claddings are oxidized by steam. This chemical reaction is highly exothermal which leads to a fast increase of temperature in the regions where oxidation occurs. When the temperature reaches the melting point of *Zr*, UO_2 pellets are partially dissolved by molten *Zr*. This has two effects on the geometry of the fuel rods : first, the pellets are no longer cylindrical and second, the molten (U - Zr - O) mixture relocates downwards, along the rods. All these mechanisms may progressively weaken the rods that may finally lose their mechanical strength and collapse into fragments. These fragments, with different size, shape and composition, form a debris bed, as it is usually called. The average "particle" diameter is of the order of a few millimetres. Fig. 1 gives a qualitative idea of the degradation processes that may occur in the reactor core if it undergoes an accidental scenario leading to a temperature escalation. The temperature of severely damaged rods and fragments may finally reach the UO_2 melting point which leads to a complete liquefaction of the core materials and the formation of a massive molten pool.

1.1 Non Uniformities in a Damaged Reactor Core

The evolution and processes described above are mainly governed by the local temperature, often in a non-linear way (i.e. creeping, oxidation and dissolution all follow Arrhenius kinetic laws). Additionally, because of the non uniform burn-up along the fuel rods and across the core, the temperature field in the core, after uncovery, is not uniform. Differences of a few hundreds Kelvin may exist between the bottom of the core and the centre. This will obviously result in differences in the local state of degradation. Those differences are amplified by the non-linear kinetic laws. A simple example is to consider rods located in the middle plane, at different radii. At the center, when the temperature reaches 1800K, which is just prior to the fast temperature escalation caused by oxidation, the rods will reach the melting point of *Zr* and UO_2 will be dissolved within a few minutes, resulting in a highly damaged geometry. On the

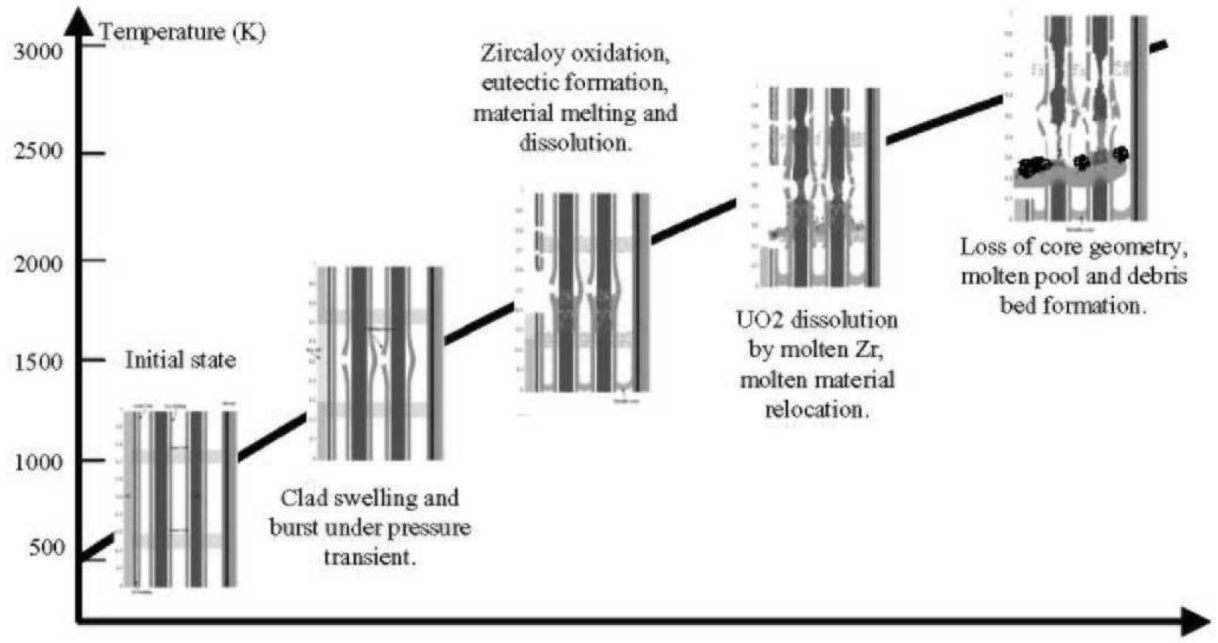

Fig. 1. Schematic View of a Nuclear Reactor Core Degradation Scenario

contrary, the external rods, which have a lower temperature may remain almost intact for a much longer time. The thermalhydraulics also induce non uniformities of the degradation. In particular, during oxidation, hydrogen is produced and accumulates downstream (i.e. at higher elevations). If steam is completely consumed, the local oxidation is stopped. This results in non uniform oxidation, even in the areas where the temperature is almost uniform. Another cause of non-uniformities is the relocation of materials, either by melting or by collapse of the rods and other structures.

Therefore severe accidents are characterized by a continuous evolution of the geometry of the core, from an initially uniform but non-isotropic medium (parallel cylinders) to a more isotropic (because of the formation of debris) but non uniform medium. In a damaged core, the porosity may vary from zero in the areas where molten materials have been accumulated to one in the cavities where rods have collapsed.

The evolution towards a more isotropic medium implies that the modelling should be at least two dimensionnal. Current codes all use a two-dimensionnal representation of the core or the vessel but not all of them actually model the heat transfers, the coolant flow and the melt progression in two dimensions. Such modeling requires the use of upscaling methods which allow to represent a complex medium as a continuous one. In this case, it must be noticed that in most parts of the reactor core, except in the cavities, the randomness of the particle distribution and the small size of the particles compared to the size of the medium allows to use homogenization methods in order to treat the damaged core as continuous medium. The purpose of this paper is to describe some models developed by the Institut de Radioprotection et de Sûreté Nucléaire (IRSN) in the last few years and integrated in the ICARE/CATHARE code in order to improve the accuracy of severe accident predictions.

1.2 Limitations of 1D Models and Transposition to the Reactor Scale

Most severe accident experiments with real materials (i.e. UO_2 and Zr) were performed at a scale which is not large enough (usually 20 rods) to be able to show significant multi-dimensional effects. Although not so fondamental at such a very small scale, the importance of multi-dimensionnal effects was however highlighted during the assessment of the first major version of the ICARE/CATHARE code (V1). The details of this extensive assessment may be found in [1] and [2]. Indeed, keeping in mind that the ICARE/CATHARE V1 code, which already included a preliminary 2-D corium relocation model, could also deal with 2-D thermalhydraulics (for single phase gaseous flow only), concurrent simulations of various SFD experiments (early or late degradation phase experiments) were therefore performed with ICARE/CATHARE at that time to compare both 1-D and 2-D modeling responses.

Comparisons between 1-D and 2-D thermalhydraulics against experiments conducted under a gas atmosphere

showed that, as soon as important rod ballooning or partial blockages appeared in the core, the radial heat transport by the fluid became important and a 1-D multi-channels model was no longer sufficient to evaluate correctly the temperatures all over the bundle. The importance of a 2-D description of the fluid flows was confirmed by the validation against both PHEBUS FPT1 rod-bundle test and PHEBUS FPT4 debris bed experiment. The FPT1 calculations showed in particular that the activation of the 2-D gaseous thermalhydraulics model allowed to better match the evolution of the cladding temperatures (and in particular the radial temperature gradient in the bundle) thanks to the correct redistribution of the steam flow from a channel to the others when a local blockage occurred. It is interesting to note that such an improvement was obtained although the convective power represented less than 20% of the nuclear power. For the FPT4 test, very good results of the thermal behaviour could be obtained only with the 2-D gaseous thermalhydraulics model.

As far as the movement and relocation of materials during the late phase of the degradation process are concerned, the simulations of the PHEBUS FPT4, ACRR-DC1, ACRR-MP1 and RASPLAV-AW- 200-4 experiments [3,4] demonstrated that, differently from the original 1-D candling model, a 2-D corium relocation model was able to properly reproduce the progression of a solid/liquid corium inside a porous medium, as well as the formation and expansion of a molten pool. Even in the early phase of the degradation process, the results obtained against the CORA-2, CORA-5, PHEBUS FPT1 and LOFT-FP-2 tests showed the global ability of both the 1-D and 2-D models to calculate the main physical phenomena occurring during the flow down of a liquid film along a solid surface such as axial relocation, heat exchanges between the corium and the solid rods, solidification of the corium and melting-solidification processes. But, unlike the 2-D model, the 1-D model was found unable to simulate the radial spreading in case of presence of an axial obstacle (blockage, plate, ...), making its application valid only to rodlike geometries. Moreover, as far as the scale effect was concerned, it was noticed that the deviations observed with the 1-D modeling, which were generally reasonable for small test bundles (20-30 rods like in PHEBUS or PBF), could become no longer acceptable for larger cores such as LOFT (120 rods), making the extrapolation of the 1-D results to the reactor conditions highly uncertain. Conversely, very promising results were obtained against the LOFT FP-2 experimental data using the 2-D corium relocation model.

In summary, although a simple 1-D multi channels approach (for both melt thermalhydraulics and relocation) could sometimes appear sufficient (case of poorly degraded small bundles), unavoidable deviations between the code simulations and the experimental data were exhibited using such a 1-D modeling in case of either small bundles more severely damaged or larger cores whatever the degradation level. Indeed, the interpretation of available SFD experimental data allowed to conclude that, the higher the degradation level is, or the larger the core size is, the more important an adequate evaluation of the fluid circulation is. So, the lack of a multi-dimensional two-phase thermalhydraulics model appeared to be prejudicial to the achievement of best-estimate reactor studies with ICARE/CATHARE V1 in case of large core blockages (no treatment of the cross-flows inside the bundle) and/or in case of a large cavity appearance (no treatment of the natural circulation). In accordance, a full multi-dimensional modeling (covering both the fluid flow and the corium behaviour) was clearly required to be developed in the next ICARE/CATHARE versions in order to be able to perform best-estimate full scale safety analyses not excluding the case of severely damaged reactor cores, with a possible late reflooding.

1.3 Outline

Although the aim of this paper is to give an overview of multi-dimensionnal models which have been proposed to calculate severe accidents, all the examples will be taken from the ICARE/CATHARE V2 code, because they were developped by the authors and they are believed to be representative of other models developped by other teams (which will be mentionned in the text). ICARE/CATHARE is developed by IRSN to be used as a tool for severe accident analysis in IRSN and other foreign institutes. Its range of applicability covers all kinds of accident sequences, from the initial phases (for instance a break in the primary circuit) to the LOCA phase and eventually to the core degradation and melting, and possible vessel failure. For that purpose, it includes all the necessary models to deal with the different physical and chemical processes involved during an accident sequence.

In a first part, the modelling of heat transfers will be described, with an emphasis on radiation which is the dominant mode of heat transfer. In the second part, the modelling of thermalhydraulics will be described, in particular during the possible reflooding of the core where multi-dimensional effects have a strong impact. In the third part, the modelling of melt progression, across the core or in the lower plenum, will be described. Finally, an accident sequence in a French PWR 900 MWe will be presented to illustrate the application of all models together in realistic conditions.

The conclusion will summarize the advantages and limitations of the multi-dimensionnal approach.

2. MODELLING OF HEAT TRANSFERS

In severe accident codes, a lot of attention must be paid to the modelling of heat transfers in the core because all the other degradation processes (oxidation, melting, relocation, FP release, etc.) actually depend on the accurate estimate of temperature. As mentionned in the introduction, the evolution towards a more isotropic medium implies that

the modelling should be at least two-dimensional. Current codes all use a two-dimensional representation of the core or the vessel but not all of them actually model the heat transfers in two dimensions. One of the simplifications made in most codes is the assumption that axial radiative heat transfers are negligible compared to radial heat transfers. However, it was shown in [5] that such an assumption is not valid in the late phase of the accident and even during the early phase in some cases. In a similar way, the radial convective transport of energy is neglected very often, because the coolant flow is assumed to be mainly 1D in the axial direction. This is also not verified in the late phase of the accident and it will be shown in the last section, presenting a complete accident scenario calculation. The heat transfer model used in ICARE/CATHARE is two-dimensional and derived from a volume averaging method, as it is explained for example in [6]. It consists in a set of energy conservation equations for the solid elements (either rods or debris), the corium melt, water and steam. For simplicity, only the equation for the corium melt is given here, under a relatively standard form:

$$\frac{\partial(\epsilon_l \rho_l \langle h_l \rangle^l)}{\partial t} + \nabla.(\rho_l \langle \vec{v}_l \rangle \langle h_l \rangle^l)$$

$$= \quad \epsilon_l \rho_l q_l + \nabla.(\mathbf{Ke} \nabla \langle T_l \rangle^l) \qquad (1)$$

$$+ h_{sl} A_{sl} (\langle T_l \rangle^l - \langle T_s \rangle^s) + h_{gl} A_{gl} (\langle T_l \rangle^l - \langle T_g \rangle^g)$$

Notations are provided in the nomenclature. **Ke** denotes the effective thermal conductivity h_{sl} and h_{gl} are the interstitial convection heat transfer coefficients *solid matrix_liquid melt* and *liquid melt_coolant fluid* respectively.

Of course, similar equations are verified for the other phases and similar coefficients must be determined as well.

As it will be shown below, the diffusion term, i.e. $\nabla.(\mathbf{Ke} \nabla \langle T_l \rangle)$ includes the effects of both conduction and radiation. It has a significant influence on the multi-dimensional heat transfers. It takes into account the geometrical configuration and the temperature. The evaluation of **Ke** is described in the two following subsections.

2.1 Radiative Heat Transfers

In severe accident codes, simple homogeneous radiative heat transfer models have been used, such as the Net Radiation Enclosure (NRE) method [7] or Hottel's method [8]. For instance, the application of those models in SCDAP and ICARE2 codes can be found in [9] or [10]. Some limitations of those models have been identified. In particular, anisotropic radiation effects must be included in the models to obtain more accurate results. This is not surprising because homogeneous models are based on the assumption of independent scattering, and cannot model properly the multiple reflections which are characteristic of the radiative transfer in a dense particle medium. Anisotropic effects can be included in homogeneous models, but it makes the determination of the optical coefficients (or the mean view factors in the case of the NRE method) very complex. Another limitation of the NRE model is that the method used to obtain the mean view factors for intact rods (i.e. Hottel's crossed strings method applied to cylinders) cannot be extended to strongly damaged rods or debris particles because of the local 3D geometry. Finally, due to the integral nature of the radiation transport equation, it is very difficult to solve in a 2D or 3D domain.

Cell models are an interesting alternative in the case of dense particle beds and, in particular, as explained by [11], the radiative conductivity model is very attractive and useful for engineering heat transfer calculations. Compared to other approaches such as the NRE method, it has the major advantage of leading to a tridiagonal system (in each direction) that is quicker to solve, because only the neighbouring meshes are coupled numerically. Moreover, this allows a straightforward extension of the model to 3D calculations. This numerical advantage and the fact that the geometry of the medium can easily be taken into account in the derivation method of the radiative conductivity are serious arguments to favour the use of this model. Therefore, it was implemented in ICARE/CATHARE, as an alternative to the standard NRE model.

It is interesting to notice that in an earlier study for EPRI, [12] had introduced the modelling of the core as a two-dimensional anisotropic porous medium made of parallel cylinders (rods) where radiative heat transfers were taken into account by introducing a two-dimensional effective conductivity. The scope of that study was limited to the early degradation phase and natural circulation effects in the core. A similar approach was later used by [13] in the DEBRIS code developed by SANDIA for the USNRC. The DEBRIS code was dedicated to the study of late phase degradation, representing the degraded core as a two-dimensional debris bed made of particles and molten materials. The ICARE/CATHARE model follows the lines explored in those earlier works and introduces a more general formulation of radiative heat transfers that is suitable for both the early and late phases of a reactor accident.

2.1.1 Radiative Conductivity

We consider that, from the initial state of the structures to the most severely degraded state, the core can be regarded as a porous medium with an opaque solid phase and a fluid phase. The intact or moderately damaged regions can be approximated by an arrangement of cylinders with a given

porosity and, according to the accident scenario, the geometry of the pores can evolve as illustrated in Fig. 1. In the porous medium that we have to describe, we assume the optically thick limit to be valid because the arrangement of particles is rather compact and their size is much lower than the size of the core. Under this condition, the net radiative flux at a particular point in space does not depend on far field effects. The local flux is only a function of local conditions and the transport rate can be described by a diffusion model, similar to Fourier's law for conduction [14]. This leads to write the radiative flux such as:

$$\mathbf{q_r} = Kr.\nabla T \tag{2}$$

where *Kr* is the *radiative conductivity* of the medium. The general form of the radiative conductivity proposed initially by Vortmeyer [15] was:

$$Kr = 4Fd_p\sigma T^3 \tag{3}$$

where d_p is a characteristic size of the particles and F is called the radiative exchange factor. Several other formulations of F can be found in the literature (see for example [15,16] or [11]).

For the geometries of interest in an intact or damaged core, the derivation of *Kr* is rather long and complex and the details are given in [17] and [18]. A general presentation of this model is also provided in [5]. The main assumptions are:

- the solid surfaces are opaque and gray and the fluid within the pores is transparent,
- the surfaces and the boundary conditions are diffuse,
- the radiative flux is not strongly anisotropic.

In the model, the non - or little - damaged reactor core is regarded as an array of parallel cylinders.

Therefore, the radiative conductivity tensor **Kr** is determined using an appropriate axis system. Figure 2 shows the selected axis system in which **Kr** becomes diagonal and can be written:

$$\mathbf{Kr} = \begin{pmatrix} Kr_\perp & 0 & 0 \\ 0 & Kr_\perp & 0 \\ 0 & 0 & Kr_\parallel \end{pmatrix} \tag{4}$$

Where, $Kr_\perp$ and $Kr_\parallel$ are the equivalent conductivities in the directions perpendicular and parallel to the cylinder array. For a damaged core, modelled as a bed of spherical particles, the tensor **Kr** is isotropic ($Kr_\perp = Kr_\parallel$).

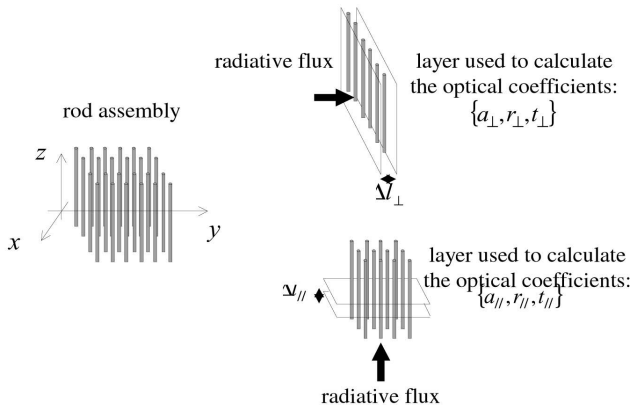

Fig. 2. Selected Axis System

When the gas is assumed to be transparent, the radiative conductivity tensor is determined by its two main components:

$$Kr_\perp = 4\left[\frac{2-(\hat{a}_\perp+2\hat{r}_\perp)}{\hat{a}_\perp+2\hat{r}_\perp}\right]\sigma T^3 d_p(\perp) \tag{5}$$

$$Kr_\parallel = 4\left[\frac{2-(\hat{a}_\parallel+2\hat{r}_\parallel)}{\hat{a}_\parallel+2\hat{r}_\parallel}\right]\sigma T^3 d_p(\parallel) \tag{6}$$

$\hat{a}$ and $\hat{r}$ are respectively the absorption and diffusion coefficients of the medium. Correlations were obtained by [17] for these optical coefficients ($\hat{a}_\parallel$, $\hat{r}_\parallel$, $\hat{a}_\perp$ and $\hat{r}_\perp$), for an array of cylinders (intact core) and for an arrangement of spheres (debris bed). The general form is the following:

$$\hat{a} = \epsilon_s n_s(p) C_a \tag{7}$$

$$\hat{r} = \epsilon_s n_s(p) C_r \tag{8}$$

where ϵ_s is the particle emissivity, $n_s(p)$ is a geometrical factor representing the effective volume occupied by a particle in a representative cell, C_a and C_r are correction factors that account for the temperature variations on the solid surfaces and the presence of neighbouring particles. They depend on the shape of the particles (cylinders or spheres) and on the geometry of the arrangement. The

details are given in [18] and [17].

2.1.2 Effective Conductivity Ke

Although the radiative heat transfers are predominant most of the time, there are cases where the thermal conductivity through the solid particles (rods or fragments) must be taken into account. In particular, at low temperature or when the porosity is low, thermal conductivity becomes the dominant mode of heat transfer. If we consider that the thermal transfer inside the porous medium is completely characterized by the radiative and the thermal conductivity tensors (**Kr** and **Kt** respectively), an equivalent conductivity tensor **Ke** may be defined as a function of **Kr** and **Kt**. In many classical approaches, and in particular for continuous methods, both heat transfer modes are considered in parallel and the equivalent conductivity is expressed as:

$$\mathbf{Ke} = \mathbf{Kt} + \mathbf{Kr}(T) \tag{9}$$

We have chosen a cell method to take into account the interaction between radiative and conductive heat transfer inside the representative cell. Fig. 3 represents a general porous medium layer in which the equivalent conductivity is obtained considering the thermal resistances associated to the following modes of heat transfer:

- the pure conduction through the free pores of the layer (*R1*) and the conduction through the solid particles (*R2*),
- the conductive transfer through the particles (contact) coupled with the radiation and the conduction in the gas phase,
- the pure radiation through the free pores of the section. This latter is decomposed in two different contributions: the radiative flux crossing the layer by direct transmission or multiple reflections (rad1) and the radiative flux absorbed and re-emitted by the particles of the layer (rad2).

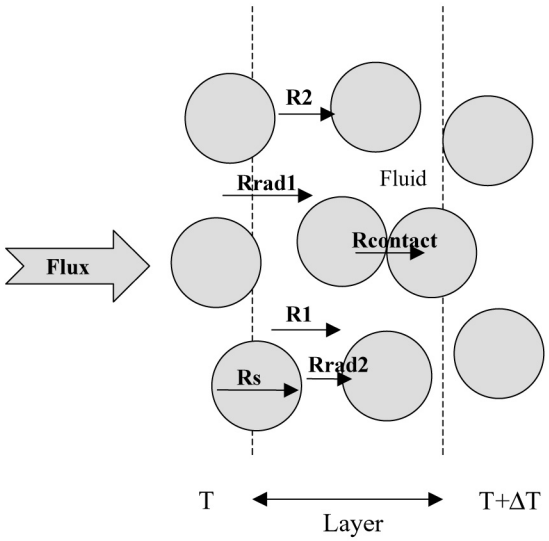

Fig. 3. Heat Transfers Through an Arbitrary Layer of Particles

The equivalent cell conductivity is expressed as:

$$Ke = k_f + Kr_{0\perp} + \frac{1}{R_S + \dfrac{1}{\dfrac{Kr_\perp - Kr_{0\perp}}{1 - R_S\left(Kr_\perp - Kr_{0\perp}\right)} + \dfrac{Kt_\perp - k_f}{1 - R_S\left(Kt_\perp - k_f\right)}}} \tag{10}$$

The details of the derivation are given in [5]. A comparison was made with several models proposed in literature [15,19,20], in particular for beds of particles which have been studied extensively. It was shown that *Ke* obtained with the present model is comparable to the values predicted by those other models. Several experiments were selected for the assessment of the ICARE/CATHARE model, mostly for particle beds: ACRR-DC1 and DC2, RASPLAV-AW, ACRR-MP1 and MP2, RASPLAV-AW and PHEBUS FPT4. The details about the calculations and comparisons with DC1 experimental data can be found in [21], where a very good agreement was obtained. A good agreement was also found for ACRR-MP1 and MP2 [22], for PHEBUS-FPT4 [23] and for RASPLAV-AW experiment [4]. For the assessment in rod geometry, Cox results [24] were found to be the only available reference. The calculations of Cox experiment with the present model may be found [5].

2.2 Particular Configurations : Cavity and Molten Pool

During the evolution of core degradation, two singular configurations may appear.

The first singular configuration is the molten pool which results from a complete densification of the medium because of melting (the porosity is zero). In this case, the radiative conductivity vanishes and the thermal part only remains, governed by natural convection and turbulent diffusion. To properly take into account natural convection, a resolution of Navier-Stokes equations is necessary. However, this requires a very fine meshing, which is not compatible with the usual CPU time requirements for severe accident computer codes. This difficulty is usually treated by using correlations for turbulent diffusion in the molten pool,

which provides the average heat transfers in the pool with a reasonable accuracy but cannot give details of the heat flux distribution along the boundaries of the pool. The turbulent thermal diffusion is introduced in the expression of **Kt** and the general formulation described above is still valid.

The second singular configuration is the large cavity which may be formed after the collapse or melting of rods (such as in TMI-2). In this case, the medium is mostly transparent and the porosity is one, which means that thermal conduction is negligible and the radiative conductivity model cannot be applied. This configuration must be treated by a different model which identifies the boundaries of the cavity. This model will not be described here because it is not as general as the others.

3. MODELLING OF THERMALHYDRAULICS

As it was mentionned in the introduction, many processes of the core degradation lead to multidimensional flows of the coolant. In particular, in the case of complete blockage of channels between the fuel rods. This has led to many studies about the coolability of a degraded core, in particular in case of reflooding.

3.1 Multi-dimensional Effects for Debris Coolability

Recently, a renewed interest has led to reconsider the conclusions that could be drawn from classical one-dimensional models such as Lipinski's. It was argued that in a debris bed formed in a reactor, the existence of heterogeneities (in porosity, debris size, power, etc...) would lead to the formation of preferential flow paths for steam and water, resulting in multi-dimensional flow patterns, far from the idealized one-dimensional situation. Experimental results [25,26] have shown that two-dimensional effects due to heterogeneities in the bed or at its boundaries may increase significantly the critical heat flux. At the same time, new two-dimensional theoretical models, such as DECO-2D [27] and WABE-2D [28,29], presented the same trends.

To treat adequately this issue, a two-dimensional two-phase flow model was developped in ICARE/CATHARE. The extension of Darcy's law for each fluid phase to describe the momentum balance equations is used. Unlike many previous models, the present one is able to take into account temperature differences between the three phases. It is also designed to calculate the flow outside the porous medium (i.e. in the possible cavities). Therefore, the tricky problem of the conditions to be applied at the boundaries of the bed is solved by using a generalized set of equations which are presented in the next subsection.

3.2 Flow Model

As it has been discussed in [29] and [30], there are still controversies about the form of the momentum equations. The volume averaging approach is difficult to use in this case because this method implies the resolution of some very complex closure problems which have only been done in simplified configurations [31]. A classical extension of Darcy's law for single-phase flow was simply used to obtain the momentum balance equations for each phase. Several simplifications have been made deliberately, compared to previous works. The exponents for the relative permeability and passability were chosen equal, as recommended by several authors [32,33,34]. The interfacial drag terms were omitted because no formulation of that term has proved to be valid over the whole range of flow parameters that may be found in our studies.

One of the first forms of momentum balance equations for debris beds was proposed by [35]. Modifications were introduced by several authors to take into account additional effects. In this study, we also take into account capillary forces and the momentum equations are written as follows:

$$\alpha\langle\rho_g\rangle^g\left(\frac{\partial\langle\mathbf{v}_g\rangle^g}{\partial t}+\langle\mathbf{v}_g\rangle^g.\nabla\langle\mathbf{v}_g\rangle^g\right)= -\alpha\nabla\langle p_g\rangle^g+\alpha\langle\rho_g\rangle^g\mathbf{g} -\epsilon\alpha^2\left(\frac{\mu_g}{Kk_{rg}}\langle\mathbf{v}_g\rangle^g+\epsilon\alpha\frac{\langle\rho_g\rangle^g}{\eta\eta_{rg}}\langle\mathbf{v}_g\rangle^g\left|\langle\mathbf{v}_g\rangle^g\right|\right) \tag{11}$$

$$(1-\alpha)\langle\rho_\ell\rangle^\ell\left(\frac{\partial\langle\mathbf{v}_\ell\rangle^\ell}{\partial t}+\langle\mathbf{v}_\ell\rangle^\ell.\nabla\langle\mathbf{v}_\ell\rangle^\ell\right)= -(1-\alpha)\nabla\langle p_\ell\rangle^\ell+(1-\alpha)\langle\rho_\ell\rangle^\ell\mathbf{g} -\epsilon(1-\alpha)^2\left(\frac{\mu_\ell}{Kk_{r\ell}}\langle\mathbf{v}_\ell\rangle^\ell+\epsilon(1-\alpha)\frac{\langle\rho_\ell\rangle^\ell}{\eta\eta_{r\ell}}\langle\mathbf{v}_\ell\rangle^\ell\left|\langle\mathbf{v}_\ell\rangle^\ell\right|\right) \tag{12}$$

In these equations, $\langle p_\beta\rangle^\beta$, $\langle\rho_\beta\rangle^\beta$, μ_β and $\langle\mathbf{v}_\beta\rangle^\beta$ are respectively the macroscopic pressure, density, dynamic viscosity and velocity of the β-phase ($\beta = g,\ l$). The macroscopic variables are defined as volume averages as in the previous section and α is the void fraction.

The capillary pressure $p_c = \langle p_g\rangle^g - \langle p_l\rangle^l$ is introduced in the equations to represent macroscopically the effect of the pressure jump across the non-wetting/wetting phase interface. It is generally modeled as a function of the saturation.

3.3 Application to Dry-out of a Particle Bed : Comparison of 1D and 2D Cases

The dryout of a submerged bed occurs when the coolant can no longer reach some parts of the bed. As the volumetric power increases, the vapor fraction within the bed increases. For a certain value of the power, the vapor flow is large enough to reduce the downward flow of the liquid to the point where it all evaporates before it reaches the bottom of the bed. The power at which this condition is just met is called the incipient dryout power and the corresponding heat flux, the critical dryout heat flux. The coolant counter-current flow also depends on the local properties (porosity, particle diameter, permeability, capillary pressure, ...). In [36] the critical dryout heat flux was determined, with the present model, for beds with different heights and particle diameters. To summarize the results, we may mention that the one-dimensional calculations well predict the dryout critical heat flux trends with respect to the particle diameter and the bed height.

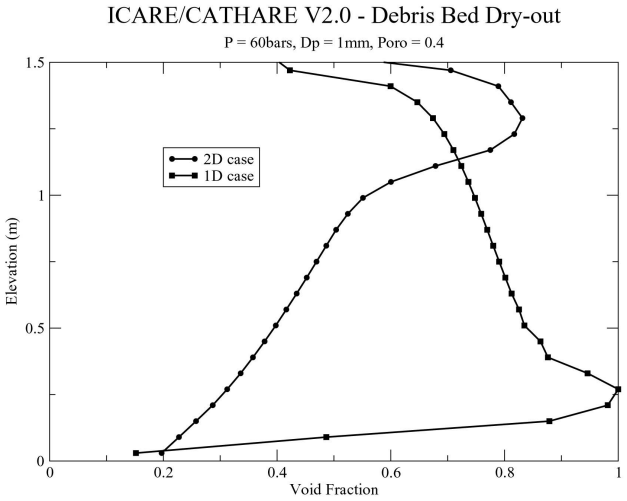

Fig. 4. Comparison of Axial Void Fraction Profile for 1D and 2D Debris Beds

To check the relevance of the 1D representation, a comparison was made between two debris beds characterized by identical parameters (particle diameter, porosity, power) but different geometries: a 1D debris bed and a 2D hemispherical debris bed (as it is expected in the lower plenum). Both beds have the same height (1.5 *m*). The power was chosen so that it leads to dry-out in the 1D configuration (330 *W/kg* of fuel). The void fraction profiles in the center of the debris bed are compared in Fig. 4. The differences are rather obvious. Contrary to the 1D situation for which dry-out starts at the bottom of the bed because liquid water cannot penetrate deeper into the bed, the 2D situation shows an accumulation of steam at the top of the bed because of gravitational effects. Such a profile may also be observed in 1D (for a lower power) but the flow pattern is completely different as it can be seen in Fig. 5: liquid water flows downwards along the vessel wall whereas steam accumulates in the upper central region where it flows upwards. As a consequence, there are no regions with strong counter-current flow which could limit water penetration into the

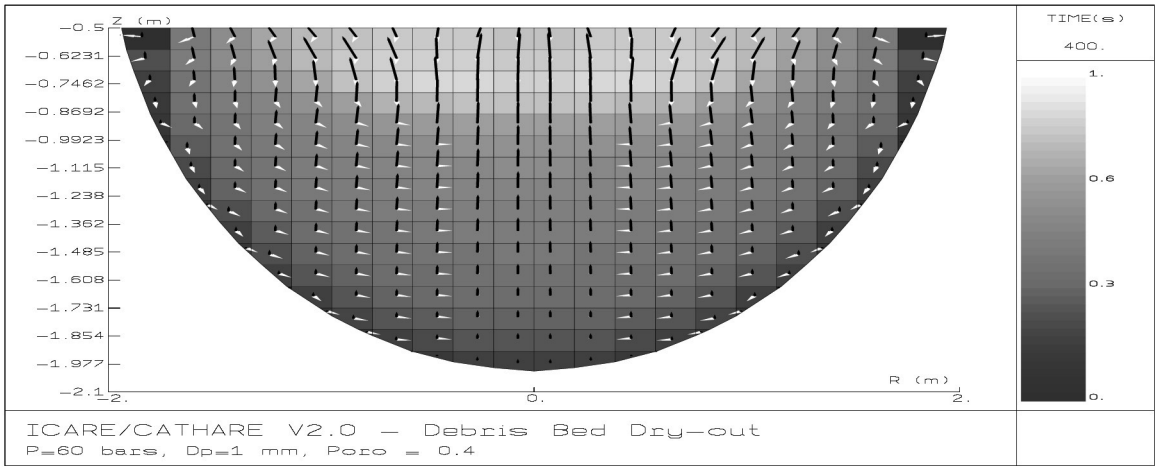

Fig. 5. Void Fraction and Velocity Fields in 2D Configuration (no dry-out) - Vector Scale : 1*cm* for 5*cm/s* (gas) or 2.5*cm/s* (liquid) - p = 60bars, d_p = 1*mm*, ϵ = 0.4

debris bed. It must be noted that the bed is perfectly homogeneous in porosity, particle diameter and volumetric power. The flow pattern and distribution of phases are only the consequence of the hemispherical geometry : the height of debris is more important in the center than on the side, therefore there is more steam generated in the center, which leads to a lower pressure in the center and a movement of the liquid towards the center, along the vessel wall. In their experimental study, [37] have observed the same phenomenon.

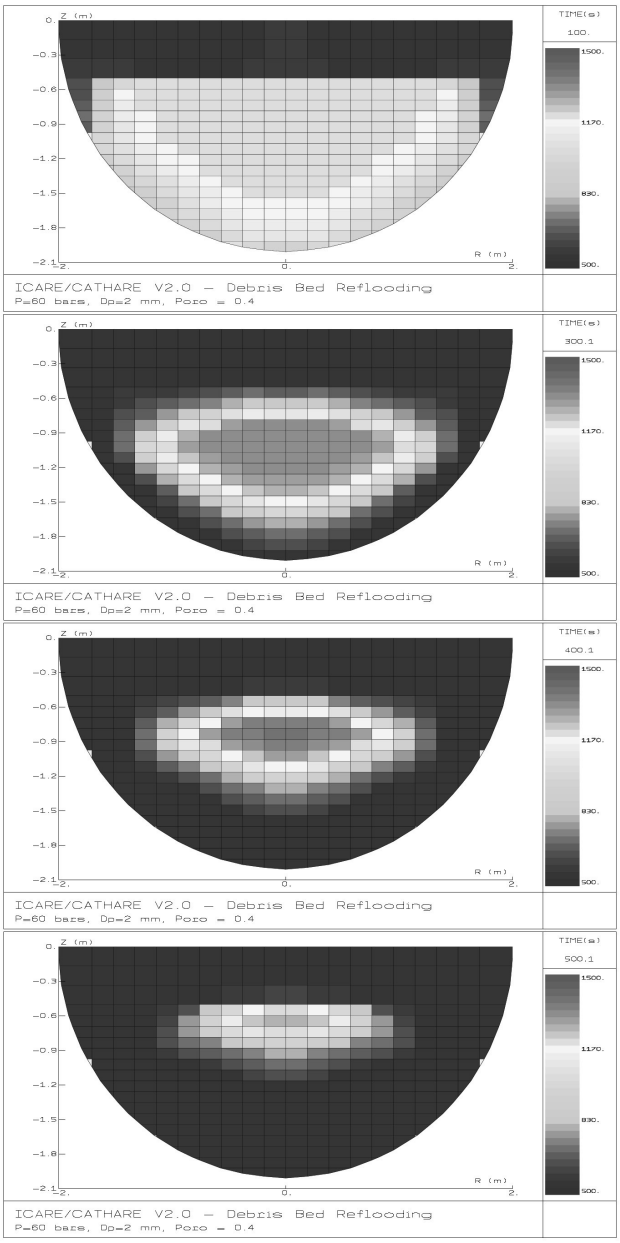

Fig. 6. Temperature Field During Reflooding (at 100*s*, 300*s*, 400*s* and 500*s*) - p = 60bars, d_p = 2*mm*, ϵ = 0.4

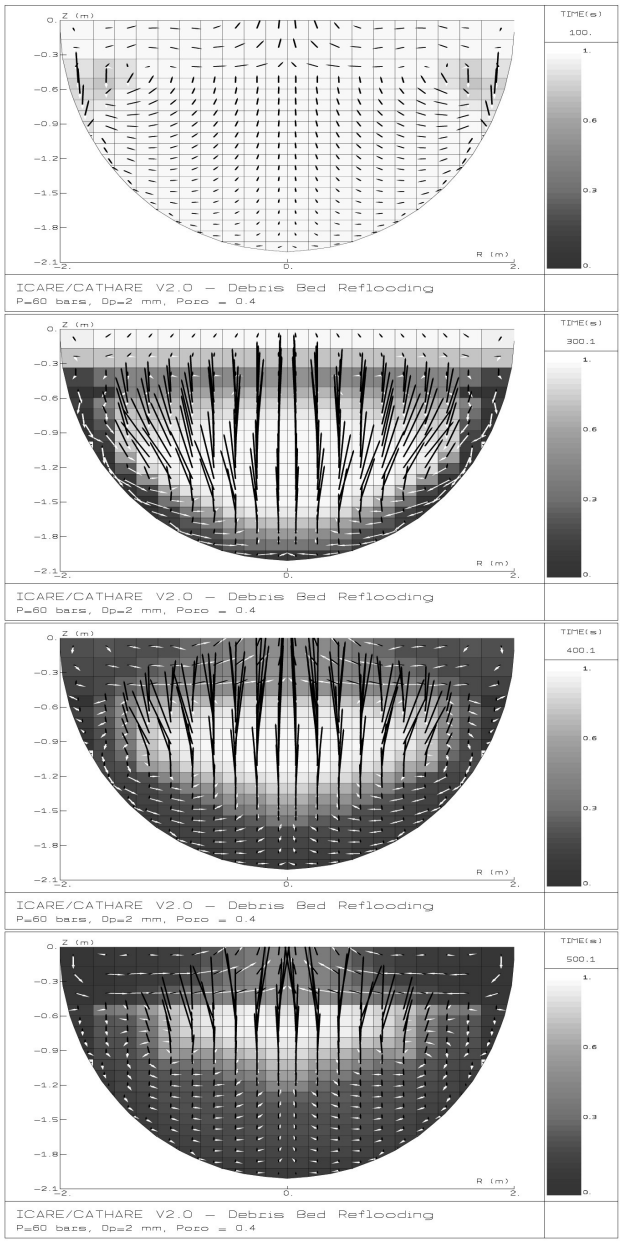

Fig. 7. Void Fraction and Velocity Fields During Reflooding (at 100*s*, 300*s*, 400*s* and 500*s*) - Vector scale : 1*cm* for 1*cm*/*s* - p = 60bars, d_p = 2*mm*, ϵ = 0.4

The consequence of that flow pattern is a higher dry-out heat flux than for the 1D configuration. This had already been predicted by other authors (see [38] for example). In fact, [39] have demonstrated experimentally that there is no limitation of the heat flux that can be removed from a debris bed as long as a sufficient liquid mass flow can enter the bed from below. The conclusion is that the accurate determination of the critical heat flux in large debris beds depends on the correct prediction of the 2D/3D two-phase flow that can be established in the debris bed. The prediction of the 2D/3D flow is also essential to estimate the time to reach the dry-out and the heat-up of the debris bed after dry-out. The main flow regime across the debris bed is characterized by a co-current flow of steam and water. After dry-out, a complex process of latent heat transport through the dry part of the debris bed leads to an efficient cooling of the debris which may remain overheated without melting. As observed by [40], there is a partial condensation of steam at the top part of the dry bubble.

3.4 Reflooding of a Particle Bed : 2D Configuration

As it was done for dry-out, we will show here how the 2D configuration changes the overall process of reflooding from what was observed in 1D experiments (or calculations).

Figs. 6 and 7 show the reflooding of a debris bed made of 2*mm* particles, with a power of 200 *W*/*kg* of fuel and a porosity of 0.4. The pressure is 60 *bar*. The initial temperature is 1050*K*, which corresponds approximately to 500*K* above the saturation temperature. Water comes from a downcomer located above the lower plenum and the debris bed. The characteristic features of the transient flow are summarized below.

- Because of the slope of the lower head, water can flow along the wall without any counter-current effect and steam escapes through the upper part of the debris bed. Moreover, the colder temperatures along the vessel wall favor a faster quenching of that region and, as it can be seen in Fig. 7, the main liquid flow path is located along the bottom wall.
- Penetration of water from the top of the bed is limited by the strong steam flow resulting from evaporation of water at the bottom. As a result, a liquid pool forms above the debris bed, and a dry “bubble” appears in the center part of the bed, where the temperature keeps increasing. This bubble is progressively quenched by water, as water is continuously driven into the bed by hydrostatic pressure difference.
- No comparison was made with 1D reflooding, but it was shown in [41] that the quenching time is significantly lower than for an assumed 1D reflooding from the top, because of the easier penetration of water into the bed. The time of quenching strongly depends on the particle size, as expected.

As for 2D dryout, it appears that 2D reflooding is mainly driven by gravity and that the total quenching time depends on the maximum mass flow of water that can penetrate into the debris bed. Water penetration is not strongly limited by steam counter-current because steam is driven out of the debris bed far from the location of water penetration. For a non homogeneous debris bed, the same process would result in the formation of dry pockets in areas with smaller particles or low porosity, while water would saturate the regions of higher permeability. If a significant fraction of the debris consists in metals (*Zr* or steel mainly), the quench front velocity and the flow path followed by steam will have a strong influence on the debris oxidation during quenching. This process was studied in [30].

4. MODELLING OF MELT RELOCATION

The relocation of (*U - Zr - O*) mixtures along the rods, resulting from cladding failure and fuel dissolution, is an important step in an accident scenario. In the late phase, the massive relocation of molten fuel mixed with other materials across porous debris is also a key process leading to the molten pool formation. A good simulation of all these events is required for a proper description of the phenomena taking place during a severe accident.

The modelling of relocation of materials outside of cylindrical tubes (i.e. fuel and control rods) is usually one-dimensional whereas the relocation across particle debris beds has been modelled in two dimensions since a long time [42,13,28]. Such works have opened a way to the elaboration of a general relocation model in ICARE/CATHARE for the flow of liquid mixture either along rods or through particles. Among the advantages of such a model is the single formulation for liquid mixture relocation either along the rods or in a porous debris bed, which simplifies the numerical resolution. Another improvement is the possibility to compute the radial spreading of corium across the rods. It is mentioned that a similar approach for two-dimensional flow in BWR assemblies had been proposed by [43] in the MERIS code.

4.1 General Model

The establishment of the conservation equations for the liquid mixture falling flow (momentum) in two directions (axial and radial-horizontal) is the main feature of this model for simulating the melt relocation. As for the thermalhydraulics model, the conservation equations are obtained with the volume averaging method. This method is especially interesting for such cases where the global interface between the fluid and the solid is complex, but may be reduced to a simple geometry when one considers a very small volume (i.e. one rod and the surrounding melt). The periodicity of the arrangement of rods or particles allows to define easily an elementary cell in which the momentum transfers can be calculated. The results of this local analysis are then used in the averaged form of the global conservation equations.

4.1.1 Liquid Mass Conservation Equation

Considering a constant density ρ_l and noting $\dot{m}_l$ the production rate of liquid corium per unit of volume, the mass conservation for the liquid is expressed by the following equation :

$$\langle \rho_l \rangle^l \frac{\partial}{\partial t} \epsilon_l + \langle \rho_l \rangle^l \nabla . (\epsilon_l \langle \mathbf{v}_l \rangle^l) = \dot{m}_l \tag{13}$$

where the filtration velocity is used:

$$\langle \mathbf{v}_l \rangle = \epsilon_l \langle \mathbf{v}_l \rangle^l \tag{14}$$

The liquid mass production rate $\dot{m}_l$ (resulting from dissolution or melting) or consumption rate (resulting from solidification) is computed independently in ICARE/CATHARE, in order to simplify the numerical resolution. However, to get more accurate results, a coupled resolution of the chemical reactions providing $\dot{m}_l$ would be necessary.

4.1.2 Momentum Conservation Equation

The volume-averaged form of the momentum equation may be found, for example, in [44]. After projecting in the direction z of the rods, one obtains :

$$\rho_l \frac{\partial (\langle v_{lz} \rangle / \epsilon_l)}{\partial t} = -\frac{\partial \langle p_l \rangle}{\partial z} - \rho_l g - \frac{\mu_l}{K^z K^z_{rl}} \langle v_{lz} \rangle - \frac{\rho_l}{\eta^z \eta^z_{rl}} \langle v_{lz} \rangle |\langle v_{lz} \rangle| \tag{15}$$

A similar equation may be obtained in the radial direction. It was shown that the form of such an equation is convenient to include several forms of friction terms. For the phemomenon under study, the most important term in the momentum conservation equation is the one coming from the generalization of the classical Darcy's law, [6], $\frac{\mu_l}{K^z K^z_{rl}} \langle v_{lz} \rangle$, due to the predominance of the viscous forces over the others. K^z and K^z_{rl} are respectively the absolute and relative permeabilities. In debris beds, the inertial forces are taken into account by the term $\frac{\rho_l}{\eta^z \eta^z_{rl}} \langle v_{lz} \rangle |\langle v_{lz} \rangle|$, where η^z and η^z_{rl} denote the passability and relative passability, respectively. These forces become significant when the velocity of the liquid mixture is large. Such a term introduces a non linearity in the resolution of the momentum equation. To make the model more general and to simplify the numerical procedure, the permeability and passability terms may be treated together according to the following transformation :

we define a drag coefficient C^z as

$$C^z = \frac{\mu_l}{K^z K^z_{rl}} + \frac{\rho_l}{\eta^z \eta^z_{rl}} |\langle v_{lz} \rangle| = \mu_l \left(\frac{1}{K^z K^z_{rl}} + \frac{Re_d}{\eta^z \eta^z_{rl} d} \right) \tag{16}$$

In the previous expression, the effect of the local Reynolds number appears clearly. More generally, to take into account the different forms of the drag coefficient for a non laminar flow regime, we may write :

$$C^z = \mu_l \left(\frac{1}{K^z K^z_{rl}} + \frac{Re_d^x}{f(s_l) d_p^2} \right) \tag{17}$$

where the exponent x may be different from 1 and f is a function taking into account the effects of the liquid film thickness around the particles. Thus, the final expression of the momentum conservation equation for the present model has the following form :

$$\rho \frac{\partial (\langle v_{lz} \rangle / \epsilon_l)}{\partial t} = -\frac{\partial \langle p_l \rangle}{\partial z} - \rho_l g - C^z \langle v_{lz} \rangle \tag{18}$$

In particle beds, many correlations are available for the permeability and the passability, which are isotropic. They may be found in [45,46] or [6] for example. The expressions proposed by [6] for the permeability in the case of flow along an assembly of cylinders are the following :

$$K^z = \frac{1}{2(d_p + 2\delta)^2} \left[\frac{d_p^2 (d_p + 2\delta)^2}{4} - \frac{d_p^4}{16} - \frac{3(d_p + 2\delta)^4}{16} + \frac{(d_p + 2\delta)^4}{4} \ln \frac{(d_p + 2\delta)}{d_p} \right] \tag{19}$$

$$K^r = \frac{(d_p + 2\delta)^2}{16} \left[\ln \frac{d_p + 2\delta}{d_p} - \frac{1}{2} \frac{(d_p + 2\delta)^4 - d_p^4}{(d_p + 2\delta)^4 + d_p^4} \right] \tag{20}$$

where δ is the thickness of the liquid corium film filling completely the space between rods which depends on the

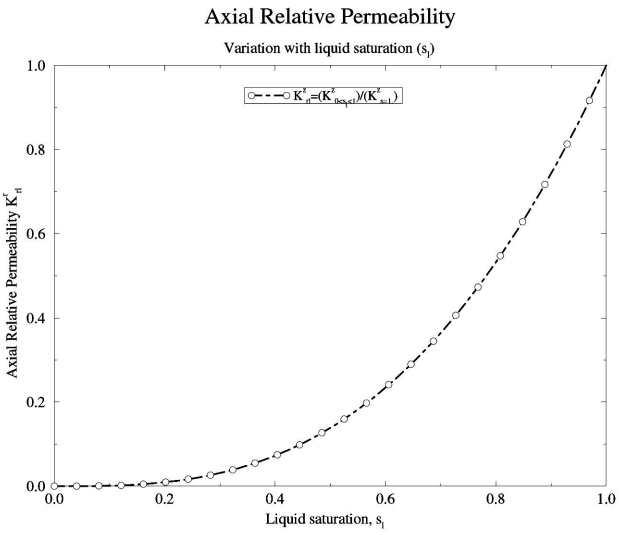

Fig. 8. Axial Relative Permeabilities as a Function of Saturation

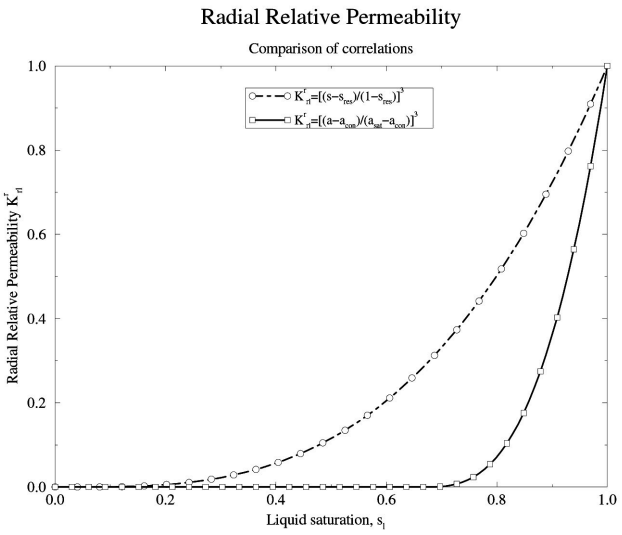

Fig. 9. Comparison of Radial Relative Permeabilities Across a Rod Bundle

geometry of the bundle and on the volume fraction of liquid melt ϵ_l.

4.1.3 Estimation of the Axial and Radial Relative Permeabilities

An analytical expression may be obtained [47] for the estimation of the relative permeability K_{rl} in the axial direction:

$$K^z_{rl} = \frac{4d_p^2(d_p+2\delta)^2 - d_p^4 - 3(d_p+2\delta)^4 + 4(d_p+2\delta)^4 \ln\dfrac{(d_p+2\delta)}{R}}{4d_p^2(d_p+2\delta_{sat})^2 - d_p^4 - 3(d_p+2\delta_{sat})^4 + 4(d_p+2\delta_{sat})^4 \ln\dfrac{(d_p+2\delta_{sat})}{d_p}} \tag{21}$$

This expression is plotted in Fig. 8.

In the radial direction, it may be assumed that there will be no radial flow as long as the liquid phase is not continuous. This means that the liquid films between neighbouring rods must be in contact ($s = s_{con}$). Under this assumption, the relative permeability in the radial direction may be expressed as follows:

- if $s < s_{con}$ $K^r_{rl} = 0$
- if $s \geq s_{con}$ $K^r_{rl} = \left(\dfrac{s - s_{con}}{1 - s_{con}}\right)^x$

where x has to be determined experimentally.

It is also possible to use a more classical approach for beds of particles, defining a residual saturation such as :

$$s_{res} = \frac{1}{86.3}\left(\frac{\sigma_l \cos\theta}{K^r \rho_l g}\right)^{0.263} \tag{22}$$

Then the relative permeability may be expressed as follows :

- if $s < s_{res}$ $K^r_{rl} = 0$
- if $s \geq s_{res}$ $K^r_{rl} = \left(\dfrac{s - s_{res}}{1 - s_{res}}\right)^x$

Both expressions are compared in Fig. 9, for a value of $x = 3$, where it appears that the radial flow is more delayed in the cylindrical geometry. This justifies the one-dimensional approach in the very early phase of the accident (limited amount of molten materials).

4.1.4 Inertial Effects

It was shown in eqs. [17] and [18] that the inertial effects can be taken into account with an additional term of the following form :

$$-\mu_l \frac{Re_d^x}{f(s_l)d^2}\langle v_{lz}\rangle = \left(\frac{\partial\langle p_l\rangle}{\partial z}\right)_{turb} + \rho_l g \tag{23}$$

From [48] it is possible to characterize the turbulent flow of a liquid film along a cylinder, with the following correlation :

$$Re_\delta = \left(\frac{\delta}{0.31\delta_{gv}}\right)^{12/7} = \frac{\rho_l \delta \langle v_{lz}\rangle^l}{\mu_l} \tag{24}$$

where $\delta_{gv} = \left(\dfrac{\mu_l}{\rho_l^2 g}\right)^{1/3}$ is the characteristic length of

gravitational-viscous interaction. After transformation of the previous expression, it may be written as :

$$\langle v_{lz}\rangle^l = -10.4\,\frac{\delta^2}{\mu_l}\left(\frac{d_p}{\delta}\right)^{3/4} Re_d^{-3/4}\rho_l g$$
$$= \frac{f(s_l)d_p^2}{\epsilon_l\mu_l} Re_d^{-x}\rho_l g \qquad (25)$$

Hence, we have $x = 3/4$ and :

$$f(s_l) = 10.4\,\epsilon s_l\left(\frac{\delta}{d_p}\right)^{5/4} \qquad (26)$$

4.2 Phase Changes: Solidification and Immiscibility

The model presented above is valid for both the rods and debris configurations (only the correlations used in the momentum equations change). However, an additional modeling difficulty is introduced because of phase changes which may affect the corium as it relocates across the core. The first phase change is solidification due to changes of composition or temperature of the melt. The second phase change is the separation in two immiscible liquids when steel is present in the mixture. This results from a miscibility gap in the quaternary phase diagram (*U - Zr - Fe - O*).

The modelling of solidification is usually made in a simple way. Considering that the flowing mixture is convectively mixed and is homogeneous in composition and temperature, one may assume that solidification will occur as a distributed nucleation of crystals inside the mixture (i.e. precipitation). In such a case, it is usual to modify the apparent viscosity μ^{eff} of the melt to take into account the transport of solid particles. Several correlations are available to calculate μ^{eff} as a function of f_s. A synthesis of the available correlations was made by [49]. μ^{eff} is a function of the temperature, which introduces a coupling between the energy and the momentum equations. This leads to implement an iterative method for the numerical resolution of the system.

The modelling of stratification is more complex and requires a coupled calculation of the thermochemical equilibrium and the phase separation. The method consists in calculating a separation velocity between the two non miscible phases according to their respective densities. This separation velocity is added to the average melt velocity obtained from the general relocation model. Because of its relative complexity, it will not be described here, but details may be found in [50].

4.3 Application to a PWR Lower Plenum Transient

A lower head configuration was chosen as an illustration in real geometry of the operation and interaction of all transport models. The interaction between the one dimensional stratification model and the two dimensional relocation model are well shown.

A French PWR-900 lower head is calculated, initially at 750K, filled with approximately 50 tons of homogeneous UO_2, ZrO_2, *Zr* and steel debris, initially at a much higher temperature (2500K). Although this is a simplified situation, these initial conditions could represent a situation following debris arrival at the lower head in the event of corium jet fragmentation and dry-out of the debris bed formed. For convenience, the lower head was supposed to be cooled on the outside by a flow of boiling water and was not allowed to fail.

Figs. 10 and 11 show the steel concentration in the corium at selected times during the simulation. The parameter plotted is the steel mass fraction in the liquid melt (multiplied by the saturation) which serves as an indicator of the presence of the metallic phase. In the presented case the metal is the heavier phase during all the transient. The colormap was set to white for very small values to give an indication of the liquid level.

The simulation begins with a debris bed and intact internal steel structures. Throughout the simulation the debris bed rises in temperature and materials successively melt (steel, then *Zr*, $Zr0_2$ and finally UO_2). Debris near the plate structures stay relatively cold (near the fusion temperature of steel) until these structures are completely molten. The central region of the lower head remains colder than its surrounding until all debris melt. Within the first 200s, thin vertical steel rods/structures surrounded by debris have completely melted and added mass to the corium while plates remain mostly intact. Although some liquid steel flows to the bottom of the lower head and refreezes, much remains in the debris itself and the liquid/debris mix remains mostly uniform throughout the debris. At about 800s, the temperature in the bulk of the debris has reached the ZrO_2 fusion temperature adding the first oxides to the liquid. At that time, the debris bed begins to lose its mostly homogenous liquid/solid mixture composition and divides into two distinct regions, a relatively liquid-free debris region and, beneath it, a liquid saturated debris region. This may be explained by the increased liquid saturation and the increased porosity (following ZrO_2 melting) which both contribute to a faster relocation of the liquid melt due to gravity. At this stage, it is interesting to notice that, despite the fact that it is lighter than UO_2,the metallic melt stays at the bottom because it fills the porosities between UO_2 particles. The size of the frozen steel region peaks around 1000s at which time the heat addition to this region from the debris begins to exceed the heat removal from this region to the lower head. Then steel melts again. This saturated debris configuration persists for a significant time with debris temperature increasing and plates melting, continuously adding steel to the liquid (Fig. 10). The upper “dry debris” region temperature rises much faster than the liquid saturated

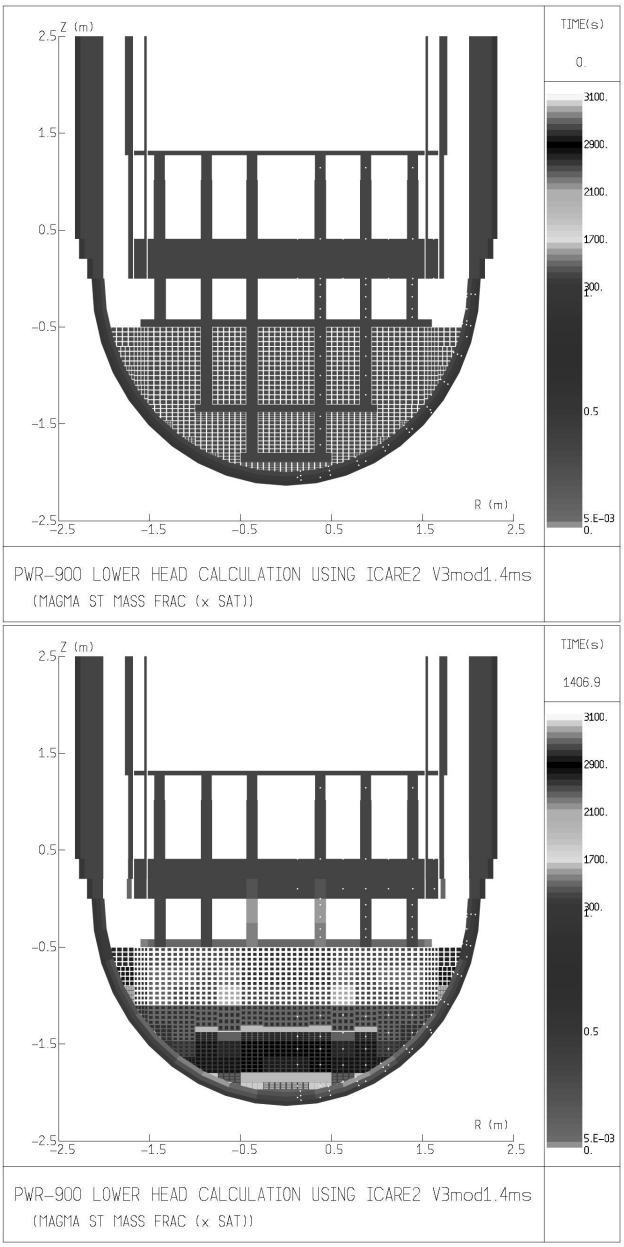

Fig. 10. Material Configuration and Steel Concentrations at 0s and 1400s. Small Squares Represent Solid Debris, the Colour Corresponds to the Debris Temperature which is Indicated on the Blue-yellow Scale. The Red-blue Scale Indicates the Steel Concentration in the Molten Materials

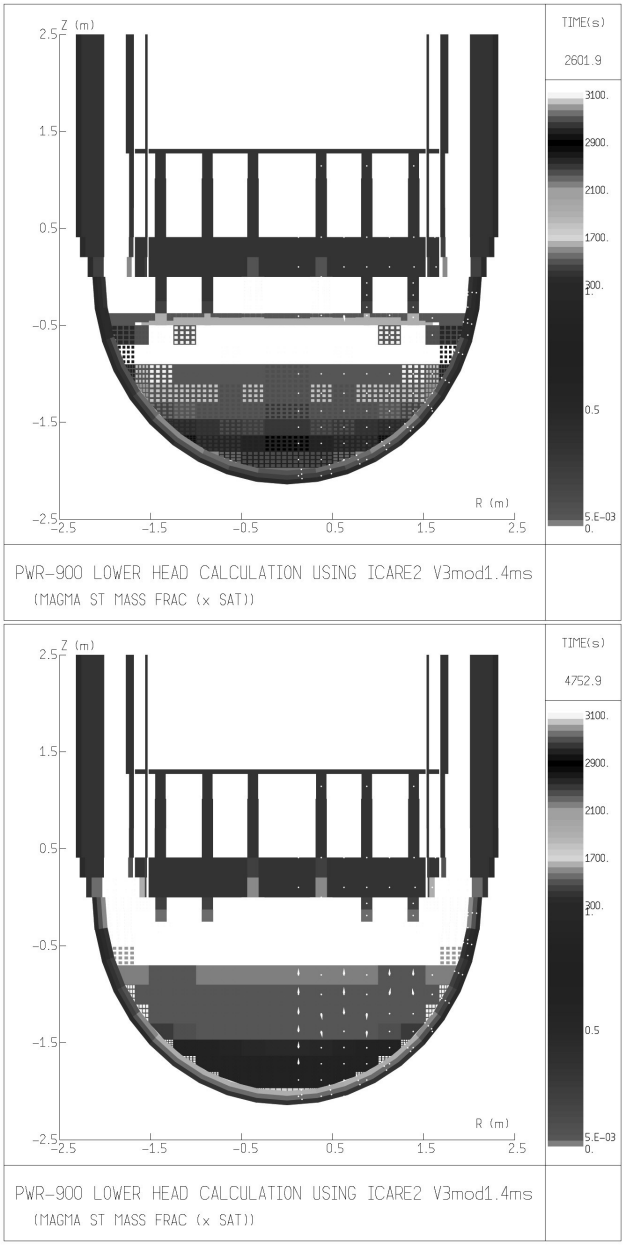

Fig. 11. Material Configuration and Steel Concentrations at 2600s and 4800s. Small Squares Represent Solid Debris, the Colour Corresponds to the Debris Temperature which is Indicated on the Blue-yellow Scale. The Red-blue Scale Indicates the Steel Concentration in the Molten Materials

debris region as less mass absorbs the energy which is almost exclusively generated in the solid UO_2. By 1800s the debris temperature has reached the melting temperature of UO_2 throughout the dry debris region except for near the vessel wall and for a slightly colder region near the plate directly above the debris. The support plate, at an elevation of -1.3m, has completely melted by this time. Large voids (cavities) develop in the liquid-free debris

region by 2000s. The elevated debris temperature results in an increase of the radiative heat transfer to the upper structures which begin to melt near this time. The bottom plate, at an elevation of -1.8m, has completely melted by 2400s. By 2600s most of the liquid free debris region has melted. Some upper structures have melted and liquid steel has collected on the plate above the debris. The upper plate ruptures soon after 3000s and is completely melted by 3600s. From 4000s on, the configuration consists of a metal/oxide stratified liquid field with a heavier metal phase. The final, stratified state at the end of the simulation at 4800s is shown in Figure 11. Solid oxides are present throughout the entire simulation.

4.4 Conclusions

The simulation presented in the previous subsection shows the necessity to calculate the progressive melting and stratification in a two-dimensional meshing to deal with such complex evolutions. It is also necessary to estimate the heat flux distribution at the boundaries of stratified molten pools. However, in the present version of the code, the calculation of heat fluxes was not implemented yet. It is also worth mentioning that the model treating the melting of debris and melt relocation (without stratification) was already assessed on several experiments such as PHEBUS-FPT4 or RASPLAV-AW-200-4 (see [4] for example) where it proved to be able to predict such processes quite accurately. An application of the relocation model to a rod bundle experiment (PHEBUS FPT1) has also shown the advantages brought by such a two-dimensional model [51]. This should be investigated further.

5. APPLICATION TO A REACTOR CASE

To better illustrate the use of all the models described in the previous section, a complete severe accident sequence in a French PWR (900MWe) is presented. It corresponds to the rupture of two steam generator tubes (SGTR) leading to core melting and relocation down to the lower plenum. All models are activated and they are solved with a semi-implicit coupling, except for melt relocation which is calculated after the temperatures have been solved.

In order to define an accidental scenario which leads the reactor core to a severe accident situation, several assumptions regarding both safety systems availabilities and operating control have been defined. The main hypothesis are to suppose both the steam generator auxiliary feed-water system and the safety injection system (high and low pressure) unavailable. This accidental transient can be divided into two characteristic steps (see Fig. 12). In the first phase which occurs just after the rupture of two steam generator tubes, primary circuit is depressurised from 155 *bar* to the secondary pressure driven by GCTA valves (76 *bar*). During this phase, there is a mass flow rate from primary to secondary circuit induced by gradient of pressure, and a loss of mass from secondary to atmosphere induced by GCTA valves. The total mass of liquid in the reactor decreases and leads to an uncovering of the core

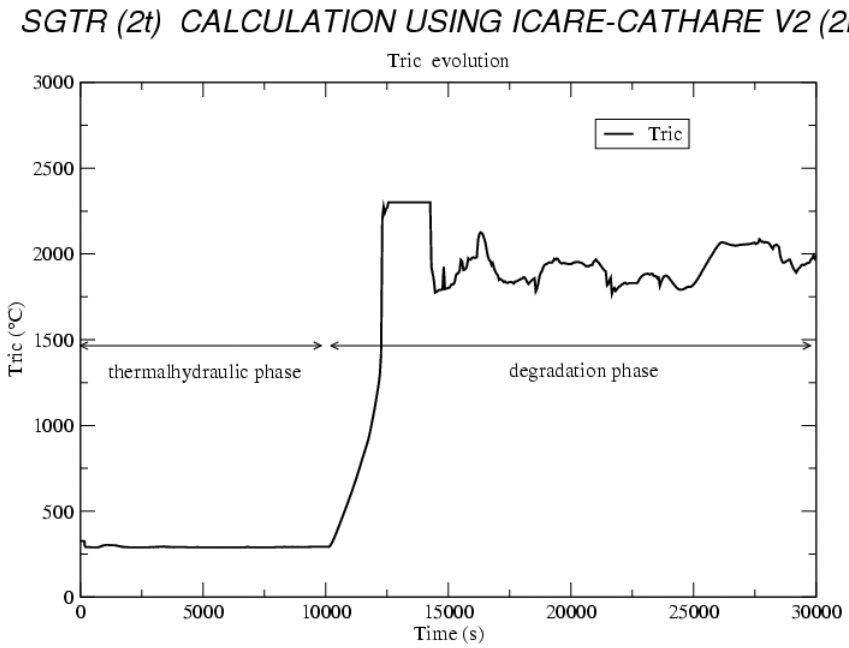

Fig. 12. Maximum Cladding Temperature as a Function of Time

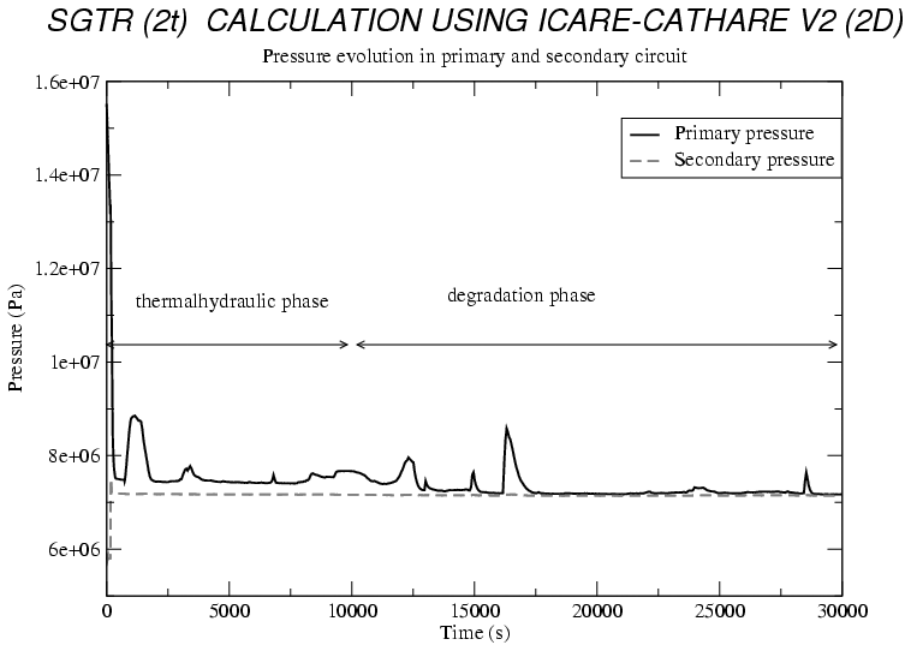

Fig. 13. Primary Pressure as a Function of Time

(second phase or degradation phase). In this second phase (10000s), the increase of the core temperatures following the core drain out leads to fuel cladding oxidation and later to a severe core degradation, with material melting and relocation (Figs. 14, 15, 16). During this phase, the peaks of primary pressure observed correspond to leakage of melting materials into the lower plenum (see Fig. 13).

The calculations clearly show the complex flow pattern resulting from the degradation in the upper part of the core and the upper plenum where two-dimensional recirculations are formed (Figs. 14, 15,16). These recirculations actually occupy all the volume located above the water level. This has a strong impact on the steam temperature at the outlet of the core and thus in the hot leg, as it was already shown in [52]. It also has a strong impact on the total hydrogen production. The melt progression is obviously two-dimensional, as it starts from the center towards the external assemblies and finally flows along the core by-pass towards the lower plenum. Since this accident sequence is just provided as an illustration, it will not be discussed further. Detailed comparisons of 1D and 2D calculations with different versions of ICARE/CATHARE (V1 and V2) are planned, in order to quantify the benefits of using 2D models.

6 CONCLUSIONS

A severe accident in a PWR is characterized by an ever changing geometry of the core with local variations of the porosity and other parameters which induce multi-dimensionnal flows and heat transfers. Although such effects are difficult to measure experimentally, the need for a multi-dimensionnal description has been widely recognized by the community of scientists in the field of severe accidents. In this paper, a comprehensive set of multi-dimensionnal models describing heat transfers, thermal-hydraulics and melt relocation in a reactor vessel was proposed. Those models are suitable for the core description during a severe accident transient when the geometry of the core evolves dramatically, due to chemical reactions, melting and mechanical failure. One important feature of those models is to separate clearly the local processes (chemical reactions, wall friction, local heat transfers) from the multi-dimensionnal transport at the large scale. This makes easier the transposition at the reactor scale of results obtained at a small scale.

Similar models were already proposed earlier or exist currently in other codes. One advantage of the ICARE/CATHARE approach is to use the same averaging method to derive each model with a consistent description. This results in a set of models which may be used in a coupled way to calculate complex sequences of a severe accident where heat transfers, thermalhydraulics and melt relocation all influence each other. The benefits of using such models has been demonstrated with several applications at the reactor scale. It shows that such detailed models, although more costly in computation time, are the only way to obtain more accurate estimates of important parameters (such as the temperature in the hot leg or the hydrogen production

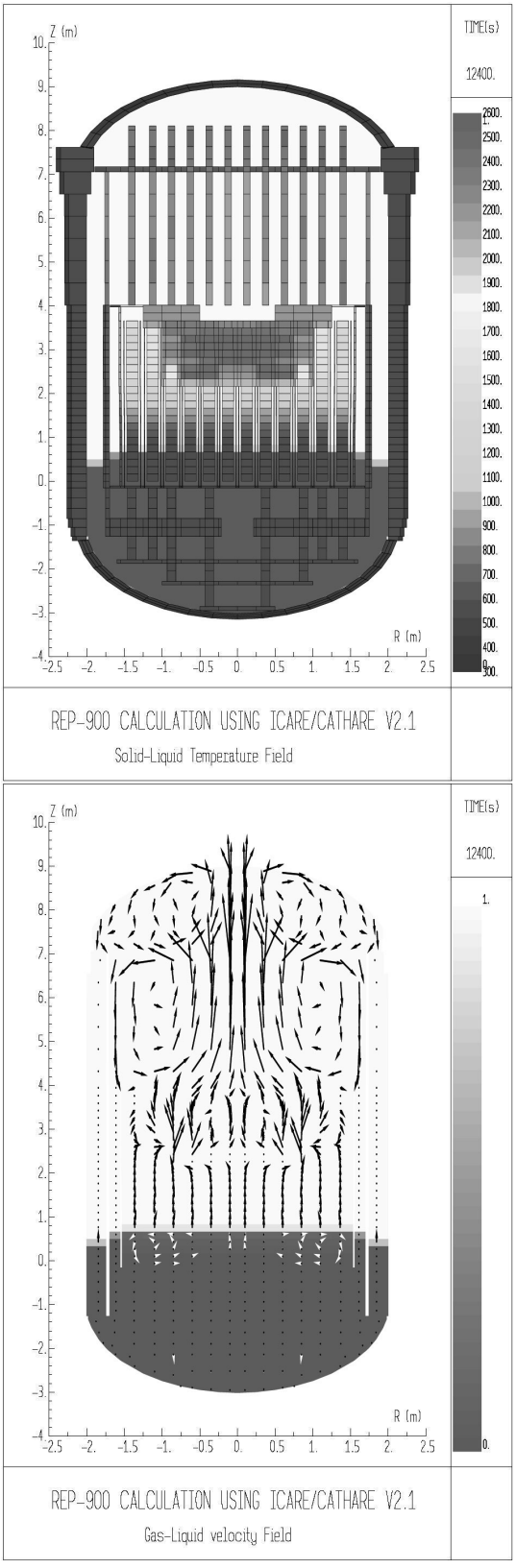

Fig. 14. State of the Vessel with Void Fraction, Velocity and Temperature at 12400s

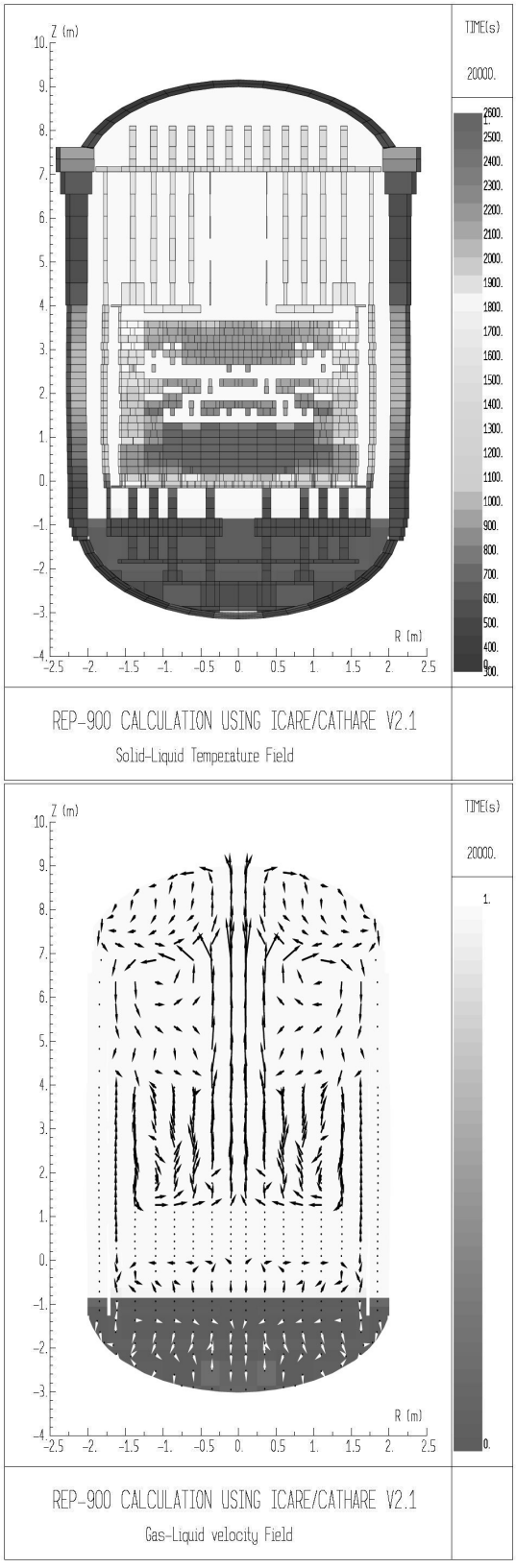

Fig. 15. State of the Vessel with Void Fraction, Velocity and Temperature at 20000s

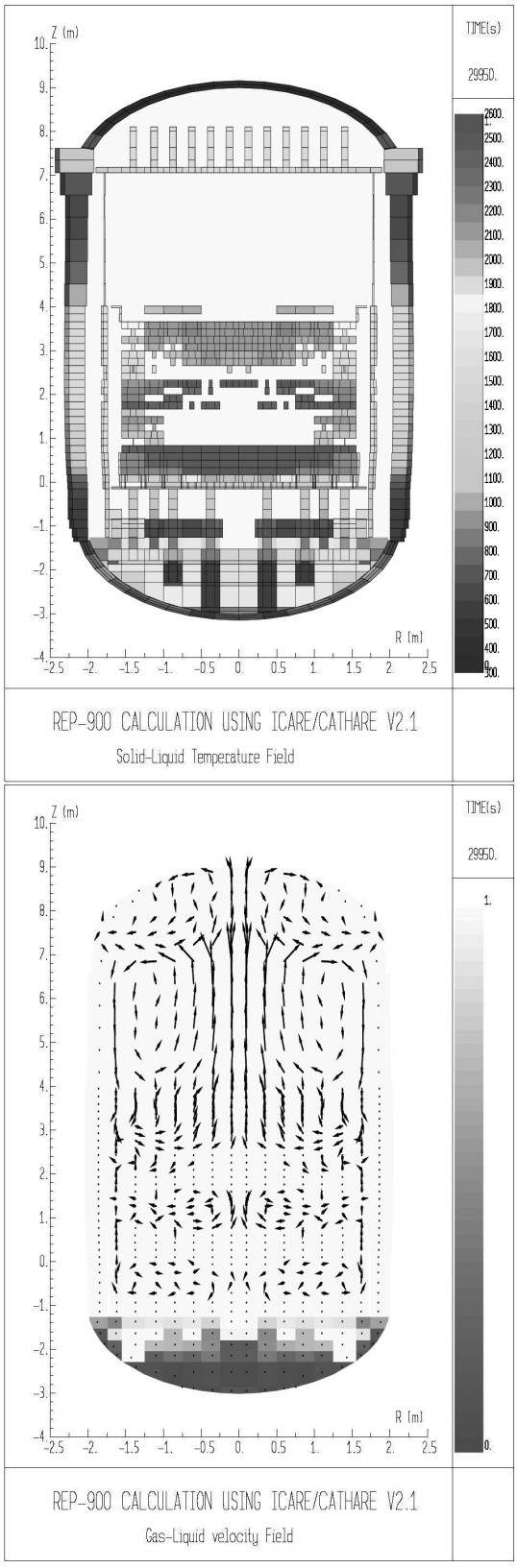

Fig. 16. State of the Vessel with Void Fraction, Velocity and Temperature at 30000s

for example) and to understand the behaviour of materials during the complex melt progression.

However, the assessment of such models is difficult because of the lack of large scale experiments. Although multi-dimensionnal models become more widely used, their development and success will rely on the design of experiments to validate them, which is one of the remaining challenges.

NOMENCLATURE

Latin letters

a	absorption coefficient
A	area m^2
d_p	particle diameter, m
h	heat exchange coefficient, $W.m^{-3}.K^{-1}$
h	specific enthalpy, $J.kg^{-1}$
K	Permeability, m^2
k	conductivity, $W.m^{-1}.K^{-1}$
Ke	Equivalent conductivity tensor
Kr	Radiative conductivity tensor
Kt	Thermal conductivity tensor
$K_{r0\perp}$	Limit of $K_{r\perp}$ when the surface emissivity tends to zero, $W.m^{-1}.K^{-1}$.
$\dot{m}$	mass rate due to phase change, $kg.m^{-3}.s^{-1}$
p	pressure, $N.m^{-2}$
q	power, $W.kg^{-1}$
r	radiative diffusivity coefficient
s	saturation, $s = \epsilon_l / \epsilon$
t	time, s
T_β	$\beta = g, l, s$, temperature in the β-phase, K
$\mathbf{v}_\beta$	$\beta = g, l$, velocity in the β-phase, $m.s^{-1}$

Greek symbols

α	void fraction
δ	liquid film thickness, m
ρ	density, $kg.m^{-3}$
μ	viscosity, $N.s.m^{-2}$
η	passability, m
ϵ_β	$\beta = g, l, s$, volume fraction of the β-phase
ϵ	porosity, $\epsilon = 1 - \epsilon_s$
σ	surface tension coefficient, $N.m^{-1}$
σ	Stefan-Boltzman constant, $5.6696.10^{-8} W.m^{-2}.K^{-4}$

Subscripts

g	gas, vapor
l	liquid
s	solid
p	particle
r	relative
$\perp$	Direction perpendicular to the vertical axis
$\parallel$	Direction parallel to the vertical axis

ACKNOWLEDGEMENT

The authors would like to thank Bertrand Lefevre, Mercedes Ortega-Bernardo and Michael Salay for their

important contributions to the development of the multi-dimensional models in ICARE/CATHARE V2.

REFERENCES

[1] P. Chatelard. Synthesis of the ICARE/CATHARE V1mod1 assessment. Note Technique SEMAR 02/07, IRSN, 2002.

[2] P. Chatelard, J. Fleurot, O. Marchand and P. Drai. Assessment of the ICARE/CATHARE V1 severe accident code. In *Proceedings of ICONE 14, 14 th International Conference on Nuclear Engineering*, Miami (USA), 2006. ASME.

[3] G. Repetto and S. Ederli. Analysis of the FPT0 and FPT2 Phebus FP experiments using porous medium geometry with the ICARE2 code. In *11th International Topical Meeting on Nuclear Reactor Thermal Hydraulics (NURETH-11)*, Avignon, France, 2005.

[4] F. Fichot, V. Kobzar, Yu. Zvonarev and P. Bousquet Mélou. The use of RASPLAV results in IPSN severe accident research program. In OECD-NEA, editor, *Proceedings of RASPLAV Seminar*, Munich, 2000.

[5] M. Zabiégo, F. Fichot and P. Rubiolo. Modeling of radiative heat transfer during a PWR severe accident. *Nuclear Technology*, 154(2):194–214, 2006.

[6] M. Kaviany. *Principles of Heat Transfer in Porous Media*. Springer-Verlag, 2nd edition, 1995.

[7] R. Siegel and J.R. Howell. *Thermal Radiation Heat Transfer*. McGraw-Hill, 1972.

[8] H.C. Hottel and A.F. Sarofim. *Radiative transfer*. McGraw-Hill Book Company, New York, 1967.

[9] M.S. Sohal. A radiation heat transfer model for the SCDAP code. *Nuclear Technology*, 75:196–204, 1986.

[10] F. Fichot, P. Chatelard, M. Barrachin, V. Guillard, S. Mélis and M. Zabièg o. ICARE/CATHARE a computer code for analysis of severe accidents in LWRs - ICARE2 V3mod1-Description of the physical models. Note Technique SEMAR 00/03, IPSN, 2001.

[11] W. Strieder. Radiation heat transport in disordered media. *Advances in Water Resources*, 20(2-3):171–187, 1997.

[12] R. Viskanta, S. Chellailah and M. Moallemi. Thermal Analysis of Core Barrel Heating and Coolant Recirculation During Core Uncovery in PWR Accidents. NP 5586, EPRI, November 1987.

[13] R.C. Schmidt and R.D. Gasser. Models and correlations of the DEBRIS late-phase melt progression model. Technical Report SAND93-3922, Sandia National Laboratories, 1997.

[14] M.Q. Brewster. *Thermal radiative transfer and properties*. Wiley-Interscience Publication, New York, 1992.

[15] D. Vortmeyer. Radiation in packed solids. In *6th International Heat Transfer Conference*, Toronto (Canada), 1978.

[16] C.L. Tien and B.L. Drolen. Thermal radiation in particulate media with dependent and independent scattering. *Annual Review of Numerical Fluid Mechanics and Heat Transfer*, 1:1–32, 1988.

[17] P. Rubiolo. *Modélisation du transfert thermique dans un milieux poreux: application aux réacteurs nucléaires en situation accidentelle*. PhD thesis, Université d'Aix-Marseille I, 2000.

[18] P. Rubiolo and J.M. Gatt. Modeling of the radiative contribution to heat transfer in porous media composed of spheres or cylinders. *Int. J. Therm. Sci*., 41:401–411, 2002.

[19] W. Schotte. Thermal conductivity of packed beds. *A.I.Ch.E. Journal*, 6:63–67, 1960.

[20] S. Imura and E. Takegoshi. Effect of gas pressure on the effective thermal conductivity of packed beds. *Heat Transfer Japanese Research*, 3(4), 1974.

[21] S. Ederli. Validation of the ICARE2 V3mod1.0 late phase models against ACRR MP-1 and DC-1 experiments. Note Technique SEMAR 01/50, IPSN, 2001.

[22] M. Le Roy and M. Zabiégo. Validation of the ICARE2 V3mod0 software against the ACRR MP-2 experiment. Technical Report 01-27, IPSN, 2001.

[23] J.C. Crestia and G. Répetto. PHEBUS FPT4: Status of post-test analysis of the debris bed behaviour with ICARE2 code. NOTE TECHNIQUE SEMAR 01/02, IPSN, 2002.

[24] R.L. Cox. *Radiative heat transfer in arrays of parallel cylinders*. PhD thesis, University of Tennessee, Knoxville, December 1976.

[25] E. Décossin. Ebullition et assèchement dans un lit de particules avec production interne de chaleur: Premières expériences et simulations numériques en situation multidimensionnelle. *Ph.D.,Institut National Polytechnique, Toulouse*, Février 2000.

[26] M.J. Konovalikhin, Z.L. Yang, M. Amjad and B.R. Seghal. On dry-out heat flux of particle debris beds with a downcomer. In *Proceedings of ICONE 8, 8th International Conference on Nuclear Engineering*, Baltimore (USA), April 2000.

[27] V. V. Likhanskii, A. I. Loboiko and V. O. Khoruzhii. Critical heat fluxes when boiling occurs in a non-uniform heat-releasing porous medium. *Atomic Energy*, 84(4):230–236, 1998.

[28] P. Mayr, M. Burger, M. Buck, W. Schmidt and G. Lohnert. Investigations on the coolability of debris in the lower head with WABE-2D and MESOCO-2D. *OECD/CSNI Workshop on In-Vessel Core Debris Retention and Coolability*, March 1998.

[29] M. Burger, M. Buck, W. Schmidt and W. Widmann. Validation and application of theWABA code: Investigations of constitutive laws and 2D effects on debris coolability. *Nuclear Engineering and Design*, 236:2164–2188, 2006.

[30] F. Fichot, F. Duval, N. Trégourès, C. Béchaud and M. Quintard. The impact of thermal non equilibrium and large scale 2D/3D effects on debris bed reflooding and coolability. *Nuclear Engineering and Design*, 236:2144–2163, 2006.

[31] M. Quintard and S. Whitaker. Transport in ordered and disordered porous media: volume-averaged equations, closure problems and comparison with experiment. *Chemical Engineering Science*, 48:2537–2564, 1993.

[32] A.E. Saez and R.G. Carbonnell. Hydrodynamic parameters for gas-liquid co-current flow in packed beds. *AIChE Journal*, 31:52–62, 1985.

[33] H.S. Lee and I. Catton. Two-phase flow in stratified porous media. In *6th Information exchange meeting on debris coolability*, Los Angeles (USA), 1984.

[34] R.J. Lipinski. A model for cooling and dryout in particle beds. Technical Report SAND 82-0765, NUREG/CR-2646, Sandia National Labs., 1982.

[35] H.C. Hardee and R.H. Nilson. Natural convection in porous media with heat generation. *Nuclear Science and Engineering*, 63:119–132, 1977.

[36] C. Béchaud, F. Duval, F. Fichot, M. Quintard and M. Parent. Debris bed coolability using a 3-D two phase model in a porous medium. In *Proceedings of ICONE 9, 9th Interna-*

tional Conference on Nuclear Engineering, Nice Acropolis, France, April 2001.

[37] P. Horner, A. Zeisberger and F. Mayinger. Evaporation and flow of coolant at the bottom of a particle-bed modelling relocated debris. *OECD/CSNIWorkshop on In-Vessel Core Debris Retention and Coolability*, March 1998.

[38] M. Buck, W. Schmidt and M. Burger. Multidimensional modelling of debris bed coolability and quenching. In *First ICARE/CATHARE Seminar*, Cadarache, France, November 2001. IRSN.

[39] F.P. Tsai, J. Jakobsson, I. Catton and V.K. Dhir. Dry-out of an inductively heated bed of steel particles with subcooled flow from beneath the bed. *Nuclear Technology*, 65:10–15, 1984.

[40] D.O. Lee and R.H. Nilson. Flow visualization in heat generating porous media. Technical Report SAND76-0614, Sandia National Labs., 1977.

[41] N. Trégourès, F. Fichot, F. Duval and M. Quintard. Multidimensional numerical study of core debris bed reflooding under severe accident conditions. In *10th International Topical Meeting on Nuclear Reactor Thermal Hydraulics (NURETH-10)*, Seoul (Korea), 2003.

[42] S.S. Dosanjh. Melt propagation in porous media. *Int. J. Heat Mass Transfer*, 32(7), 1989.

[43] R.C. Schmidt. MERIS: a model for melt relocation in core structures of nuclear reactors during severe accident conditions. Technical Report NRC FIN L-2452, Sandia National Laboratories, 1993.

[44] S. Whitaker. Flow in porous media II: The governing equations for immiscible, two-phase flow. *Transport in Porous Media*, 1:105–125, 1986.

[45] F. A. L. Dullien. *Porous Media Fluid Transport and Pore Structure*. Academic Press, Inc., 1979.

[46] A.E. Scheidegger. *The Physics of Flow Through Porous Media*. University of Toronto Press, 1974.

[47] F. Fichot, M. Ortega-Bernardo and B. Lefevre. Melt relocation through a rod bundle. Note Technique SEMAR 99/34, IPSN, 1999.

[48] S. S. Kutateladze. *Handbook of Heat Transfer and Hydrodynamical Resistance*. Energoatomizdat, 1990.

[49] M. Ramacciotti. Modèles de viscosité des systèmes contenant des particules en suspension. Etude bibliographique. Note Technique 98/056, CEA/DER/SERA/VULCANO, 1998.

[50] M. Salay and F. Fichot. Modelling of corium stratification in the lower plenum of a reactor vessel. In OECD/NEA, editor, *Proceedings of OECD MASCA Seminar*, Aix en Provence (France), June 2004.

[51] M. Ortega-Bernardo and F. Fichot. Post-test calculations of FPT1 test using ICARE2 V3MOD0 code : an alternative scenario. In *Proceedings of ICONE 8, 8th International Conference on Nuclear Engineering*, Baltimore (USA), April 2000.

[52] V. Guillard, F. Fichot, P. Boudier, M. Parent and R. Roser. ICARE/CATHARE coupling : three-dimensional thermalhydraulics of LWR severe accidents. In *Proceedings of ICONE 9, 9 th International Conference on Nuclear Engineering*, Nice Acropolis, France, April 2001.